07,05

Phase composition and magnetic properties of boron-doped $Fe_{75}C_{25}$-based alloys: mechanosynthesis, annealing

© A.A. Chulkina, A.I. Ulyanov, A.L. Ulyanov, A.V. Zagainov

Federal State Budgetary Scientific Organisation Udmurt Federal Research Center
of the Ural Branch of the Russian Academy of Sciences,
Izhevsk, Russia

E-mail: chulkina@udman.ru

Received November 10, 2025
Revised November 12, 2025
Accepted November 15, 2025

A structural and phase analysis of boron-doped cementite $Fe_{75}(C_{1-x}B_x)_{25}$ alloys with $x = 0.05, 0.1, 0.2$ and 0.4 was performed using X-ray diffraction, magnetic measurements, and Mössauer spectroscopy, both after mechanical synthesis and after subsequent annealing. The features of carbide phases alloying in these alloys were investigated. During the mechanical synthesis process, cementite is minimally alloyed with boron. When annealed above 400 °C, the boron concentration in this phase increases significantly. The Curie temperature of cementite in $Fe_{75}(C_{1-x}B_x)_{25}$ alloys annealed at 800 °C increases with increasing boron content, ranging from 210 to 360 °C. In alloys with increased boron content $Fe_{75}(C_{0.8}B_{0.2})_{25}$ and $Fe_{75}(C_{0.6}B_{0.4})_{25}$, when annealed at temperatures above 600–650 °C, part of the borocementite is transformed into the boron-doped phase $Fe_{23}(C,B)_6$, the Curie temperature of which after annealing at 800 °C is 450 and 480 °C, respectively.

Keywords: mechanosynthesis, annealing, phase composition, carbides, boron alloying.

DOI: 10.61011/PSS.2025.12.63084.319-25

1. Introduction

The materials of tools for cutting and processing steel products and minerals must simultaneously withstand high mechanical loads, have increased hardness and low wear. Modern tool steels are a strong and viscous matrix containing solid carbide phases. The production of tool steels based on carbide phases requires expensive doping elements such as W, Cr, V, Co, Mo and others. To reduce the cost of tool steel production, researchers are increasingly paying attention to boron, since its alloys with iron have a hardness close to or higher than hardness of chromium carbide Cr_7C_3 (1500–1600 HV), which is a commonly used hard phase in tool steels. For example, the hardness of boride Fe_2B is 1600–1700 HV [1], and the hardness of FeB is up to 2000 HV [2], however, this boride very brittle. However, borides, in comparison with carbides, have a number of other useful properties, such as higher values of heat resistance and modulus of elasticity [3,4].

The optimal ratio of hardness and viscosity is realized on triple Fe–B–C alloys. Due to the low solubility in the iron lattice [5], a small amount of boron is sufficient to form a significant volume of hard phases. It was experimentally shown in Ref. [6], that the hardness of ternary alloys, in particular, borocementite $Fe_3(C,B)$, increases with increasing boron content.

The study of phase formation in cast alloys of the system (Fe–C–B), as well as the measurement of their hardness, was performed in Refs. [7–9]. It should be noted that the Fe–B–C system has not yet been fully studied. It was noted in Ref. [8] that there are disagreements about the mechanisms of formation and the region of stability of the phase $Fe_{23}(C,B)_6$.

It was shown in Ref. [8] that α-Fe nuclei are primarily formed during the primary crystallization of alloys of the pre-eutectic Fe–C–B alloys and Fe dendrite growth occurs on the basis of these nuclei. In this case, the residual melt is enriched with B and C atoms. When the temperature decreases to 900–1000 °C, in alloys with a high boron content, in addition to the hard phase $Fe_3(C,B)$, a small amount of Fe_2B may be present, that is, the microstructure of the alloys is characterized by primary Fe dendrites surrounded by a eutectic structure of hard phases. In the temperature range of 700–800 °C, a peritectoid transformation of the $Fe_3(C,B)$ phase occurs according to the schematic reaction $Fe_3(C,B) + Fe \rightarrow Fe_{23}(C,B)_6$ or the reaction of decomposition of $Fe_3(B,C) \rightarrow Fe_{23}(C,B)_6 + Fe_2B$ occurs at higher ratios of B/(C+B). With an increase in the boron content, the $Fe_{23}(C,B)_6$ phase forms a shell around the $Fe_3(B,C)$ and/or Fe_2B phases, which prevents further decomposition of the $Fe_3(C,B)$ phase. Thus, depending on the local B/(C+B) atomic ratio and the heat treatment temperature, hard phases Fe_2B, $Fe_3(C,B)$ (hardness up to 1400 HV) and $Fe_{23}(C,B)_6$ (hardness up to 1400 HV) can be simultaneously present in cast steels.

When the boron content exceeds 1 wt.%, the hard phase of high-boron iron-carbon alloys forms a continuous network along the iron grain boundaries, which leads to a decrease in the fracture toughness of the alloys [10]. Such an alloy Fe–C–B is no longer suitable for tools operating under high impact loads. To improve the wear resistance of highly boron alloys, it is necessary to break the chains of

hard phases and disperse them into a binding matrix. This problem was solved in Ref. [10] by using thermomechanical treatment. The problem of morphology of hard phases can be solved if alloys are prepared using powder metallurgy, hot isostatic pressing, or liquid phase sintering [11,12]. A significant disadvantage of such technologies is their high cost, high sintering temperatures, and coarse-grained (on the order of tens — hundreds μm) alloy structure.

Currently, it has been proven that materials with grain sizes in the nanometer range possess the highest strength characteristics [13]. The nanostructured state of massive materials is usually obtained by intense plastic deformation by high-pressure torsion or equal-channel angular pressing [14]. However, such methods are of little use for hard boron-containing steels. At the same time, the nanostructured state, including that of hard alloys, is relatively easily obtained by mechanical alloying (MA) of powders of the initial components in ball planetary mills [15]. Special compaction methods are needed for the practical use of such powder materials that would not destroy their nanocrystalline state. Nevertheless, it is convenient to conduct fundamental research on nanostructured powders, for example, the effect of doping elements, thermal and other treatments on the structural and phase state, thermal stability and physical properties of the studied alloys.

There are reports in the literature on mechanosynthesis in ball planetary mills of nanocrystalline boride phases [16,17]. However, studies of nanocrystalline alloys in the Fe–C–B system were clearly insufficient. It is worth noting the study in Ref. [18], in which compact nanocomposites based on mechanosynthesized powders of the compositions $Fe_{75}(C_{1-x}B_x)_{25}$ and $Fe_{83}(C_{1-x}B_x)_{17}$ ($x = 0.2$ and 0.4) were produced. After sintering, the alloys contained hard phases of carbides $Fe_3(C,B)$ and $Fe_{23}(B,C)_6$, and ferrite as the binding phase. The size of the precipitates of carbide phases and ferrite was in the nanometer or submicron range. The porosity of the samples was at the level of 16–20 %.

This paper continues to study the properties of boron-containing nanocomposites. The issues of formation, doping, and changes in the structural state of solid nanocrystalline phases in the processes of mechanosynthesis and subsequent annealing of boron-doped alloys based on $Fe_{75}C_{25}$ are discussed.

2. Samples and research methods

The mechanosynthesis of alloys of the $Fe_{75}(C,B)_{25}$ composition was performed in a ball planetary mill „Pulverisette-7“ in an argon atmosphere. The energy intensity of the mill was 2 W/g. The milling balls and grinding vessels were made of steel ShH15. The alloys were produced from carbonyl iron powders with a purity of 99.98 and graphite with a purity of 99.99 %. Alloy powders of the composition Fe — 8.53 wt.% B were chosen as the boron source, which is close to the composition of the Fe_2B phase. The time of mechanosynthesis of the initial powders was reduced to 8 h to reduce the wear of the grinding bodies during the MS process. Annealing at a temperature of 800 °C of alloys in the stage of incomplete (MS time 8 h) and completed mechanical alloying (after 16 h of MS) leads to almost the same phase formation according to the data in Ref. [18], but with a lower iron content from grinding balls and vessels, which was no more than 3–4 % of the mass of the initial powder. The ratio of the mass of grinding balls with a diameter of 10 mm to the mass of powders was $\sim 9:1$.

Hour-long annealing of mechanosynthesized powder samples was performed in an argon atmosphere at a facility for measuring the temperature dependence of relative magnetic susceptibility $\chi(T) = \chi_T(T)/\chi_{20}$. Here χ_T is the current magnetic susceptibility value obtained at a measuring temperature T normalized to the value of χ_{20} measured during heating at a temperature of 20 °C. The Curie temperature T_C of the ferromagnetic phases of the alloys was estimated from the dependences $\chi(T)$ determined during heating and cooling of the samples at a rate of 30 deg/min. The frequency of the probing alternating magnetic field with an amplitude of 1.57 Oe was 120 Hz.

X-ray diffraction patterns were obtained at a room temperature using „Miniflex 600“ diffractometer (Rigaku, CoK_α-radiation, Bragg-Brentano geometry, velocity 2 deg/min). Quantitative X-ray diffraction analysis, as well as precision determination of the cementite lattice parameters, were performed using the software package [19].

The Mössbauer spectra were measured at a room temperature using SM2201DR spectrometer in the transmission geometry in the mode of constant accelerations of the source of γ-radiation of ^{57}Co(Rh). Annealed carbonyl iron powder was used as a standard absorber. Mathematical processing of the spectra in order to restore the function $P(H)$ of the distribution of hyperfine magnetic fields on the nuclei of the ^{57}Fe isotope was performed in a continuous representation using a generalized regularized Tikhonov algorithm for solving inverse incorrectly-posed problems [20]. The Lorentz line sextet (single-core model) was used as the core of the Fredholm integral equation.

The magnetic characteristics of the samples were measured on a vibrating magnetometer with a maximum magnetizing field of 16 kOe.

3. Results and their discussion

$Fe_{75}(C_{1-x}B_x)_{25}$ samples with $x = 0.05, 0.1, 0.2$ and 0.4 being the proportions of carbon atoms replaced by boron atoms were prepared to study the effect of boron content on the formation of the structural-phase state and temperature stability of boron-containing phases of alloys. For brevity, we will futher refer the fraction of boron atoms in the alloy as x. The same alloys in atomic representation can be written as $Fe_{75}C_{25-y}B_y$, where $y = 1.25, 2.5, 5$ and 10 at. %. Figure 1 shows typical diffraction patterns of alloys $Fe_{75}(C_{0.95}B_{0.05})_{25}$ and $Fe_{75}(C_{0.8}B_{0.2})_{25}$, and Table 1

Table 1. X-ray phase composition of the studied alloys. The phase composition data of alloys after annealing at $T_{ann} = 500\,^{\circ}C$ are given without taking into account the XAP*, since it is not possible to correctly identify this phase due to the content close to the error of its determination

Alloy composition	T_{ann}, °C,	CXAP, vol.% ±2	Ferrite, vol.% ±2	$Fe_3(C,B)$, vol.% ±2	$Fe_{23}(C,B)_6$, vol.% ±2	Fe_2B, vol.% ±2
$Fe_{75}(C_{0.95}B_{0.05})_{25}$	MC	34	19	45	–	**2**
	500	–	5	95	–	–
	800	–	2	98	–	–
$Fe_{75}(C_{0.9}B_{0.1})_{25}$	MC	30	16	49	–	**5**
	500	–	10	90	–	–
	800	–	8	92	–	–
$Fe_{75}(C_{0.8}B_{0.2})_{25}$	MC	38	15	44	–	3
	500	–	8	92	–	–
	600	–	6	94	–	–
	650	–	2	88	10	–
	800	–	–	81	19	–
$Fe_{75}(C_{0.6}B_{0.4})_{25}$	MC	46	15	27	–	12
	500	–	13	83	–	4
	600	–	2	89	9	–
	800	–	1	77	22	–

Note. * XAP — disordered X-ray amorphous phase.

shows the phase composition of the studied alloys in the state after MS and subsequent annealing, obtained from the analysis of X-ray diffraction patterns. Additional information about the doping of ferromagnetic phases can be obtained from magnetic measurements, as well as Mössbauer studies.

It is known that when ferromagnetic phases of alloys are heated or cooled, peaks or inflection appear on the temperature dependence curve of the relative magnetic susceptibility $\chi(T)$ in the region of their Curie temperature (T_C) (Hopkinson effect). Information about T_C makes it possible to quickly identify ferromagnetic phases, as well as assess the degree of their doping with boron. Figure 2 shows the dependences $\chi(T)$ of low-boron alloys $Fe_{75}(C_{0.95}B_{0.05})_{25}$ (Figure 2, *a*) and $Fe_{75}(C_{0.9}B_{0.1})_{25}$ (Figure 2, *b*) and alloys with high boron content $Fe_{75}(C_{0.8}B_{0.2})_{25}$ (fig. 2, *c*) and $Fe_{75}(C_{0.6}B_{0.4})_{25}$ (Figure 2, *d*). For ease of perception, the curves of dependences $\chi(T)$ of each alloy annealed at various temperatures up to 800 °C are shown in the same figure with the vertical offset of axes „*T*“ and „χ“Ṫhe axes „*T*“ (for $\chi = 0$) for each dependency are represented in the figures as horizontal dotted lines with the designation „0_n“ (on the right), where n is the curve number.

It follows from Figure 2 that the curves of dependences $\chi(T)$ of the studied alloys have a lot in common, but there are also differences. The curves *1* reflect the phase transients that occur during continuous heating of alloys. The peak of the curve *1* indicates the transition through the Curie point, that is, from the ferromagnetic to the paramagnetic state, of the cementite and the X-ray amorphous phases formed during the MS process, T_C of which slightly differ. The X-ray amorphous phase in this case is a disordered phase that begins to form in the interface zone between the grains of nanocrystalline α-Fe and has the appearance of an amorphous halo on X-ray diffraction patterns. We will further denote this phase as XAP. The presence of cementite and XAP in alloys after MS is confirmed by X-ray diffraction analysis data (Table 1).

The curves *2*–*8* in Figure 2 are measured during the cooling of samples after one-hour annealing at various temperatures T_{ann}. It can be seen that the Curie temperature T_C of cementite of almost all alloys with the annealing temperature of up to $T_{ann} = 400\,^{\circ}C$ is close to T_C of the undoped cementite (210 °C) (curves *2*). Consequently, the doping of cementite alloys with boron in this range of T_{ann} is minimal. The exception is the alloy $Fe_{75}(C_{0.6}B_{0.4})_{25}$. Figure 2, *d* shows that the peak of the curve *2* is blurred, and T_C of the cementite of this alloy is located near $\approx 224\,^{\circ}C$. This means that a certain number of boron atoms have already been dissolved in the cementite of the $Fe_{75}(C_{0.6}B_{0.4})_{25}$ alloy annealed at $T_{ann} = 400\,^{\circ}C$.

The presence of only a small number of boron atoms in cementite, formed both during the MS process and during annealing up to $T_{ann} = 400\,^{\circ}C$, may be attributabe to the peculiarity of boron as an doping element. Boron is poorly soluble in α-Fe. The solubility of boron in α-Fe is very small in the equilibrium system of Fe–B and amounts to 0.001 at.% at $T = 500\,^{\circ}C$ according to Ref. [5]. In addition, the low reactivity of boron during mechanical alloying was found in Refs. [21,22], which leads to its extremely slow dissolution and complicates its participation in the amorphization process. It is noted in Ref. [21] that, there are significant differences despite some similar processes in the kinetics of phase formation in the binary systems Fe–C and Fe–B. Let us compare the MS processes of alloys

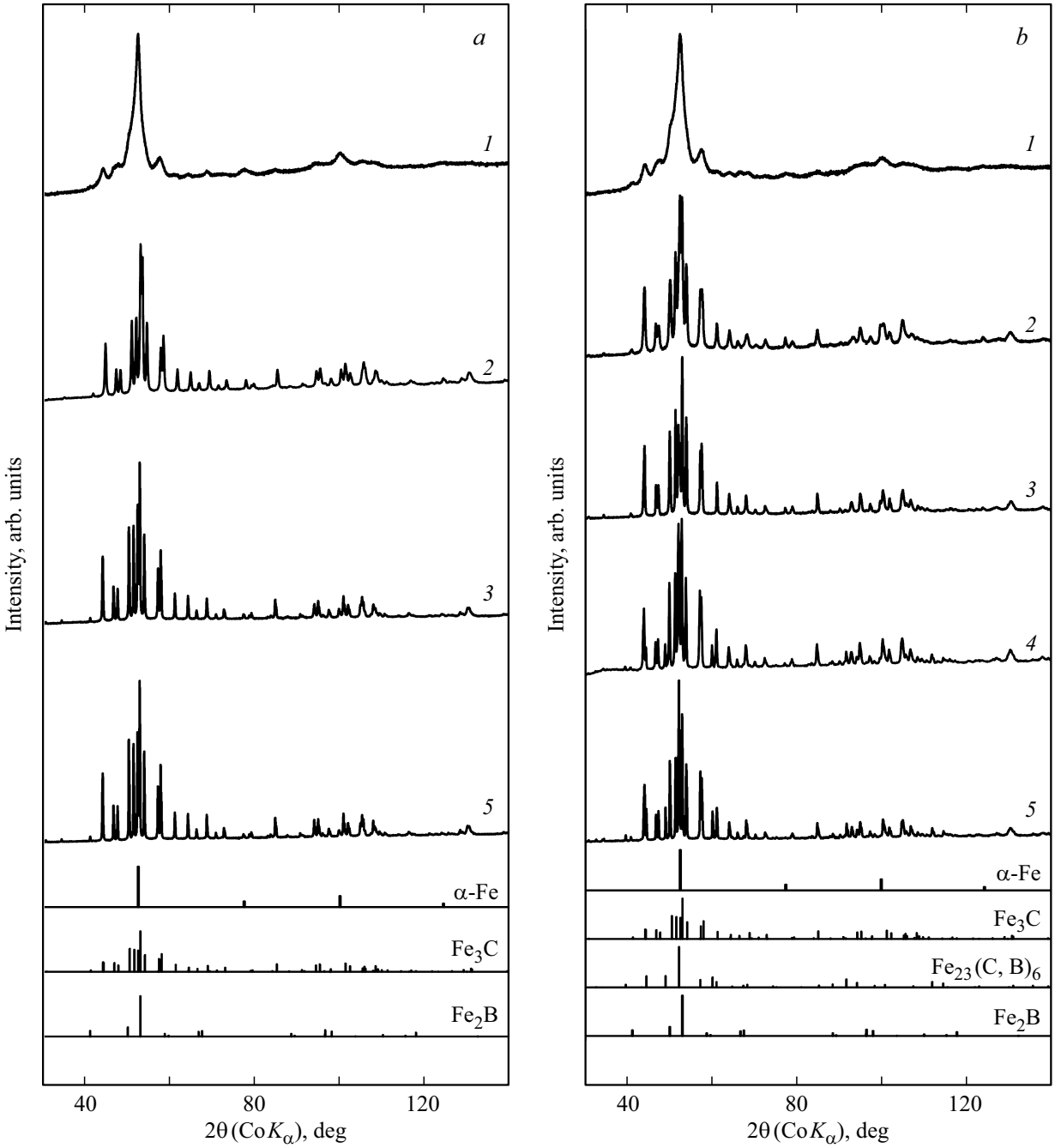

Figure 1. Alloy diffraction patterns: *a* — $Fe_{75}(C_{0.95}B_{0.05})_{25}$, *b* — $Fe_{75}(C_{0.8}B_{0.2})_{25}$after *1* — MS and subsequent annealing at *T*, °C: 500 (*2*), 600 (*3*), 650 (*4*) and 800 (*5*).

$Fe_{85}B_{15}$ and $Fe_{85}C_{15}$ described in this paper. According to the authors, the segregation of carbon and boron atoms is formed in the grain interface boundaries of α-Fe nanograins at the initial stage of mechanosynthesis. Moreover, the kinetics of the formation of segregations of these atoms in α-Fe particles is approximately the same: 3.7 at.% carbon and 4.5 at.% boron are concentrated in segregations at the boundaries of α-Fe after 4 h of MS. XAP is formed and grows in the interface zones at the second stage of MS. The formed segregations of C and B atoms are sources of metalloid atoms in the XAP. It was found that the rate of release of boron atoms from the segregations in the XAP is significantly lower than the rate of release of carbon atoms. This is evidenced by the fact that after MS for 8 h, the amount of formed XAP in $Fe_{85}B_{15}$ alloy is almost two times less than in $Fe_{85}C_{15}$ alloy. Accordingly, up to 4 at.% B and only 1.5 at.% C remain in the segregations. The authors attribute the low mobility of boron atoms compared to carbon in the MS and phase formation processes to the different covalent radii of B and C atoms (0.88 and 0.77 Å,

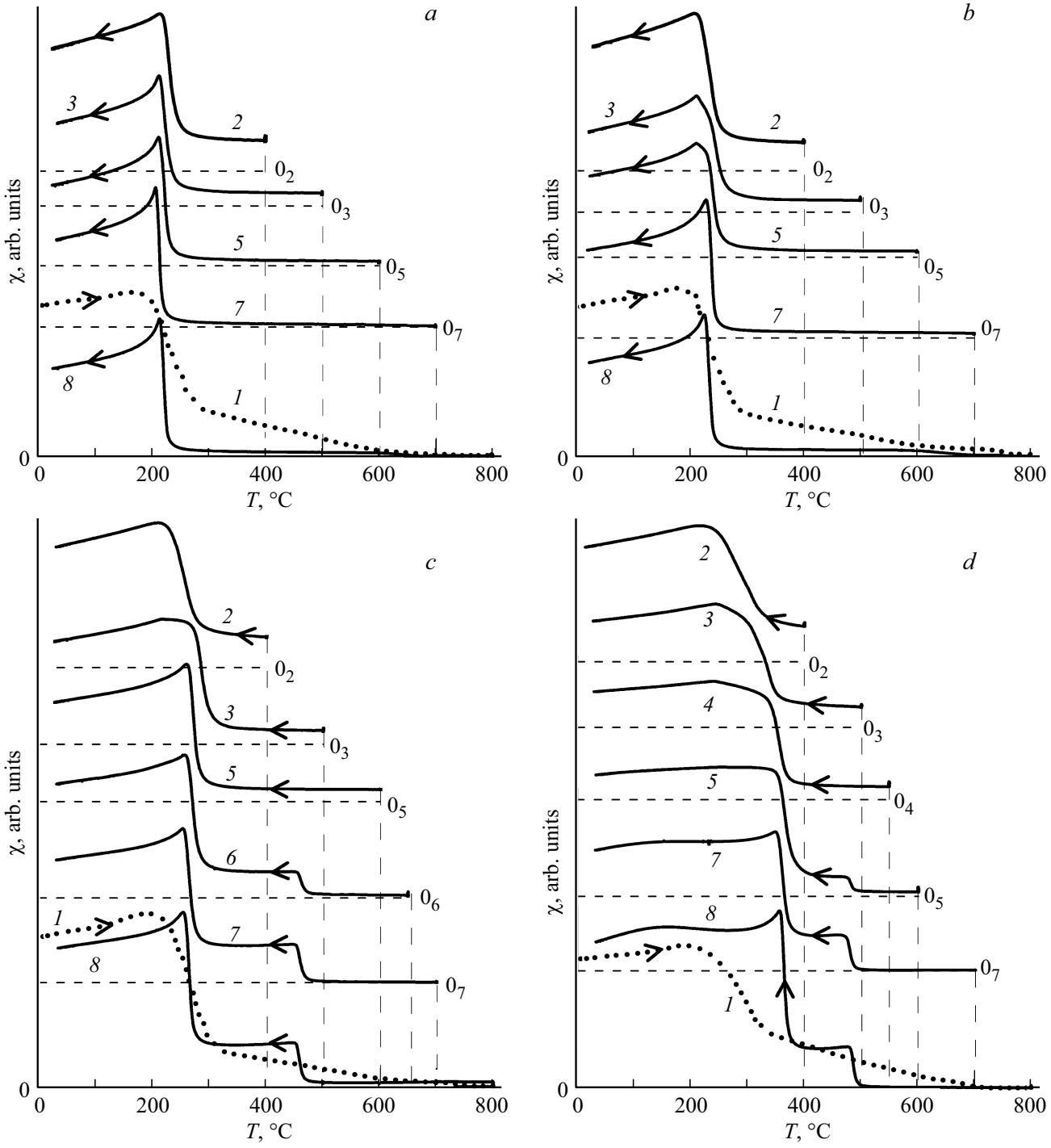

Figure 2. Temperature dependences of the relative magnetic susceptibility of $\chi(T)$ alloys: *a* — $Fe_{75}(C_{0.95}B_{0.05})_{25}$, *b* — $Fe_{75}(C_{0.9}B_{0.1})_{25}$, *c* — $Fe_{75}(C_{0.8}B_{0.2})_{25}$, *d* — $Fe_{75}(C_{0.6}B_{0.4})_{25}$ measured when heated after MS (*1*) and cooled after annealing at T_{ann}, °C: 400 (*2*), 500 (*3*), 550 (*4*), 600 (*5*), 650 (*6*), 700 (*7*) and 800 (*8*).

respectively). Thus, it can be assumed that the XAP of the alloys studied in this paper will consist mainly of Fe and C atoms after 8 h of MS (the MS equipment is similar to that used in Ref. [21]). A small amount of the X-ray amorphous phase is formed with the participation of boron atoms. Part of the boron-depleted XAP is converted into cementite in the MS process. In this case, the residual segregation is located mainly along the boundaries of XAP [23], and may also be adjacent to the boundaries of cementite grains.

It should also be noted that nonstoichiometry of the composition [24,25], associated with point defects, is often observed in carbide phases. In mechanosynthesized

cementite, the predominant point defects are vacancies in those lattice sites where metalloid atoms should be located. Not all metalloid atoms, especially of large covalent radius, manage to break out of segregation in the MS process. However, this is possible in case of annealing. However, carbon atoms, as a result of their overwhelming majority and high mobility, primarily fill the bulk of the vacant metalloid lattice sites of cementite in the studied alloys, especially low-boron ones, during annealing up to $T_{ann} \approx 400\,^{\circ}C$. The low-boron part of the XAP is actively converted into cementite in the annealing process at such temperatures. A significant part of the boron atoms still remain in the segregation along the boundaries of the residual XAP and cementite grains.

As is known, the solubility of boron in cementite strongly depends on the temperature [26,27]. Boron is able to replace up to 80 % of carbon at 1000 °C and about 60 % of carbon at 600 °C. Therefore, it should be expected in this study that the solubility of boron in cementite will begin to increase with an increase in $T_{ann} > 400\,^{\circ}C$ of alloys, which was found experimentally. $Fe_{75}(C_{0.9}B_{0.1})_{25}$, $Fe_{75}(C_{0.8}B_{0.2})_{25}$ and $Fe_{75}(C_{0.6}B_{0.4})_{25}$ alloys, which can be represented as $Fe_{75}C_{22.5}B_{2.5}$; $Fe_{75}C_{20}B_5$; $Fe_{75}C_{15}B_{10}$, contain 2.5, 5 and 10 at.% of boron, respectively. An „influx" appears on the right side of the maximum of dependences $\chi(T)$ after annealing at 500 °C (Figure 2, *b*–*d*, curves *3*). The „influx" becomes more capacious with a further increase in T_{ann}. And after annealing at $T_{ann} = 700-800\,^{\circ}C$, it turns into an acute, pronounced peak at temperatures of 224, 255 and 360 °C, characterizing T_C of the boron-doped cementite (borocementite) alloys with a B content of 2.5, 5 and 10 at.%, respectively (Figure 3).

The content of boron in the segregation and XAP of the low-boron alloy $Fe_{75}(C_{0.95}B_{0.05})_{25}$ in the post-MS state is low. Therefore, cementite will be weakly doped with boron at annealing temperatures above 500 °C, that is, at the end of the process of crystallization of residual boron-doped XAP and dissolution of the segregations. This is

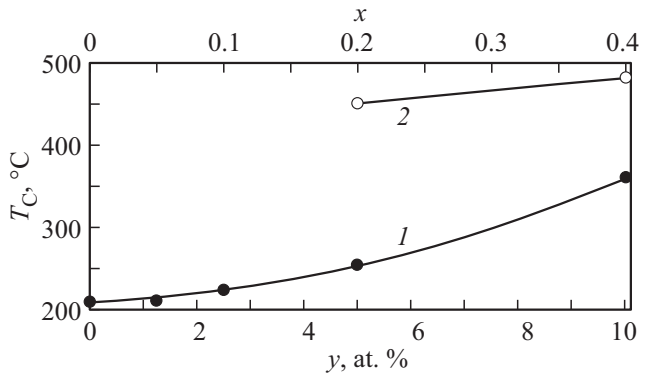

Figure 3. Curie temperature dependence T_C of boron-doped phases of $Fe_3(C,B)$ (*1*) and $Fe_{23}(C,B)_6$ (*2*) on the atomic content of boron in $Fe_{75}C_{25-y}B_y$ alloys or on the fraction of x of boron atoms in the same $Fe_{75}(C_{1-x}B_x)_{25}$ alloys. The alloys were annealed at 800 °C.

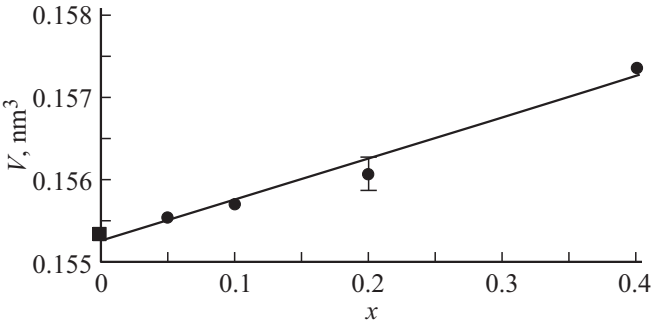

Figure 4. Dependence of the cell volume of cementite on the fraction of boron atoms x in $Fe_{75}(C_{1-x}B_x)_{25}$ alloys annealed at $T_{ann} = 800\,^{\circ}C$. The data for the MS-alloy $Fe_{75}C_{25}$ ($x = 0$), due to its temperature instability during annealing at $T_{ann} = 800\,^{\circ}C$ [29], were taken for a sample annealed at $T_{ann} = 500\,^{\circ}C$(1 h) from Ref. [30].

evidenced by the Curie temperature of cementite of such an alloy, which practically does not change with increase of the annealing temperature and is close to T_C of undoped cementite (Figure 2, *a*).

Let us check the atomic composition of the cementite formed during the MS and annealing processes, based on the data of its Curie temperature obtained in this study. The results of measuring of T_C of cementite in cast alloys depending on the content of both boron and carbon in it are provided in Ref. [26]. Unfortunately, any later studies with data on T_C of $Fe_3(C,B)$ cementite were not available. Based on the data from Ref. [26], we estimated the atomic composition of cementite MS alloys. For example, borocementite with $T_C = 360\,^{\circ}C$ has an atomic composition of $Fe_3(C_{0.62}B_{0.38})$, which is close to the atomic composition of the alloy studied in this paper $Fe_{75}(C_{0.6}B_{0.4})_{25}$.

Boron stabilizes cementite. As follows from the calculations in Ref. [28], Fe–Fe bonds weaken as a result of an increase of the volume of the cementite cell with an increase in the concentration of boron in it (confirmed by experimental results obtained in this work (Figure 4)). At the same time, the stability of cementite increases due to the formation of significantly stronger Fe–B covalent bonds compared with weak Fe–C bonds. A change in the sign of the enthalpy of formation ΔH, which indicates the stability of the compound, is observed near the composition $Fe_{75}(C_{0.8}B_{0.2})_{25}$ (if $\Delta H < 0$, then the compound is more stable than the simple substances from which it was formed, if $\Delta H > 0$ — then vice versa). Nevertheless, as can be seen from Figure 2, *a* and Table 1, even weak boron doping of cementite alloy $Fe_{75}(C_{0.95}B_{0.05})_{25}$ significantly increases its temperature stability (within the studied temperature range) in contrast to the undoped cementite alloy $Fe_{75}C_{25}$, some of which decomposes at elevated temperatures of heat treatment [29].

Let's continue the discussion of Figure 2. On the dependence curves $\chi(T)$ obtained after annealing alloys with a high boron content $Fe_{75}(C_{0.8}B_{0.2})_{25}$ and $Fe_{75}(C_{0.6}B_{0.4})_{25}$

(Figure 2, *c* and *d*) at $T_{ann} \geq 600-650\,^{\circ}C$, in addition to the maximum characterizing T_C borocementite, there are well-marked inflections at temperatures of 450 and 480 °C, respectively. These inflections reflect T_C of the new phase, which, according to Table 1, can be attributed to the phase $Fe_{23}(C,B)_6$ (Figure 3, curve *2*). As follows from Ref. [8], the stable temperature range for the formation of the phase $Fe_{23}(C,B)_6$ is in the temperature range of $600-950\,^{\circ}C$. The temperatures of formation of $Fe_{23}(C,B)_6$ obtained in this study practically fit into this range.

The presence of ferrite (α-Fe) in alloys after MS and annealing can be qualitatively judged by the values of the relative magnetic susceptibility χ, determined in the measurement temperature range above T_C of carbide phases (Figure 2), and it can be quantitatively determined by the X-ray diffraction analysis (Table 1). Mössbauer studies can also confirm the data on the phase composition of the studied alloys, as well as provide information on the doping of phases with boron.

The Mössbauer spectra of the studied alloys in the state after MS and subsequent annealing are shown in Figure 5 (left). The functions $P(H)$ reconstructed from the spectra are shown in the same figures (on the right). These functions reflect the probability density of the distribution of hyperfine magnetic fields on the nuclei of ^{57}Fe isotopes from the atoms of the nearest environment. The type of functions $P(H)$ of the main phases of alloys of the Fe–C system is known. For example, the function $P(H)$ of undoped cementite Fe_3C has a peak corresponding to an hyperfine magnetic field on the nuclei of iron isotopes $H = 205-207$ kOe [30,31]. For α-Fe (and also ferrite), the maximum of the function $P(H)$ lies in the field $H = 330$ kOe [32]. In alloys of the Fe–C system prepared by mechanosynthesis, XAP usually has a function distribution of $P(H)$ over a wide range of magnetic fields H from ≈ 100 to 300 kOe [32]. The type of function $P(H)$ changes in case of a phase doping.

It follows from the curves *1* in Figure 5 that in the post-MS state, the functions $P(H)$ of alloys exhibit a pronounced maximum at $H = 330$ kOe, which pertains to ferrite. It is difficult to separate the functions $P(H)$ of an unreacted Fe_2B alloy ($H = 235-240$ kOe [33]), weakly doped cementite and XAP. The separate maximum in the field of $H = 110$ kOe is also visible on the curves *1* of the function $P(H)$. However, it is impossible to attribute it to another phase, since there are no additional phases in the composition of the MS samples according to the results of the X-ray diffraction analysis (Table 1). Since the Mössbauer studies provide information not about the long-range, but about the short-range order of the atoms surrounding the resonant isotopes of ^{57}Fe, it can be assumed that the maximum in the field $H = 110$ kOe belongs to the XAP alloys. Indeed, it has been shown in a number of studies that the function $P(H)$ of some amorphous boron-containing alloys obtained by spinning has two maxima of the function $P(H)$, one of which is located in the region of weak magnetic fields H. This type of function $P(H)$ was obtained in Ref. [34] on fast-quenched strips of Fe–B alloys with a boron content of 12–14 at.% (Figure 6) and in other papers in Refs. [35–37] studying boron-containing alloys. The authors explain the appearance of two maxima of the function $P(H)$ by the heterogeneous distribution of metalloid atoms in the immediate environment of Fe atoms. Based on this information, we assume that the function $P(H)$ of the X-ray amorphous phase of the studied alloys after mechanosynthesis is a wide distribution of an hyperfine magnetic field in the range from 160 to 300 kOe, which overlaps with the functions $P(H)$ of cementite and Fe_2B, as well as the distribution with a small maximum in the field of $H \approx 110$ kOe. Thus, it can be concluded that MS alloys really consist of cementite, ferrite, XAP and a small amount of Fe_2B.

The structural and phase changes occurring during annealing and observed in the thermomagnetic dependences $\chi(T)$ (Figure 2) should also be reflected in the functions $P(H)$ of phases of alloys. Common to all studied alloys is the fact that XAP is intensively transformed during annealing, which should lead to a decrease and then disappearance of the function $P(H)$ of this phase, in particular, in the range of H from 90 to 120 kOe, which is really what is happening (Figure 5). As a result of the crystallization of XAP, as well as the decrease in the density of defects in the crystal structure during annealing at $T_{ann} > 500\,^{\circ}C$ and the removal of distortions of crystal lattices, the maxima of the functions $P(H)$ of phases become narrower and more pronounced (Figure 5).

Phases are doped with boron during MS and annealing, which should be reflected in the Mössbauer spectra and, consequently, in the shape and position of the maxima of the functions $P(H)$ of phases. The maximum of function $P(H)$ of cementite lies practically in the same fields of $H = (206 \pm 3)$ kOe for the low-boron $Fe_{75}(C_{0.95}B_{0.05})_{25}$ alloy both after MS and subsequent annealing to 800 °C (Figure 5, *a*). The presence of a narrow symmetrical peak of the function $P(H)$ in these fields after annealing of the alloy at $T_{ann} > 500\,^{\circ}C$ indicates the minimum content of boron atoms in the immediate environment of iron atoms located in cementite. The effect of boron doping of cementite begins to manifest itself on the alloy of $Fe_{75}(C_{0.9}B_{0.1})_{25}$. Figure 5, *b* shows that near the maximum of its function $P(H)$, additional components form from the side of higher fields H, which form the asymmetry of the peak of the function $P(H)$ of cementite. Moreover, the asymmetry persists even after high-temperature annealing. It was shown in Ref. [38] that the hyperfine magnetic field of H increases linearly with an increase in the magnetic moment of Fe atoms in various iron carbides. It follows from this that the formation of additional components from the side of higher fields of H can be explained, according to the data from Ref. [39], by an increase in the magnetic moment of iron atoms with an increase in the concentration of boron atoms in the cementite lattice.

Mössbauer spectra and functions $P(H)$ of alloys with high boron content (Figure 5, *c* and *d*) are similar in many

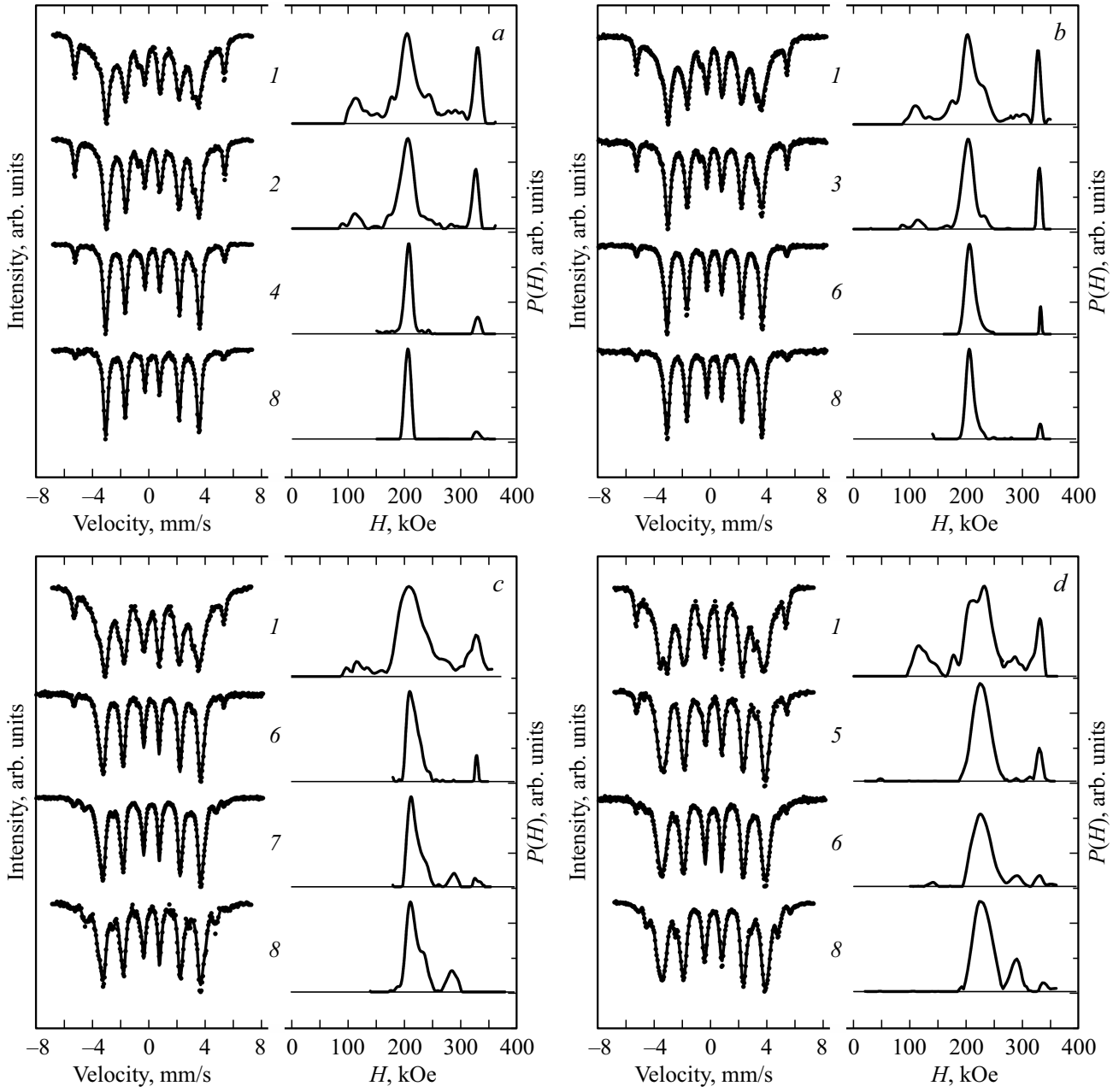

Figure 5. Mössbauer spectra and functions of $P(H)$ alloys $Fe_{75}(C_{0.95}B_{0.05})_{25}$ (*a*), $Fe_{75}(C_{0.9}B_{0.1})_{25}$ (*b*), $Fe_{75}(C_{0.8}B_{0.2})_{25}$ (*c*) and $Fe_{75}(C_{0.6}B_{0.4})_{25}$ (*d*) after MS (*1*) and subsequent annealing at temperatures of T_{ann}, °C: 300 (*2*), 400 (*3*), 500 (*4*), 550 (*5*), 600 (*6*), 650 (*7*) and 800 (*8*).

ways to the previous ones, but there are also differences. Due to the appearance of a significant number of boron atoms in cementite alloys, the maxima of the function $P(H)$ widen. At the same time, the hyperfine magnetic field H of borocementite alloys $Fe_{75}(C_{0.8}B_{0.2})_{25}$ and $Fe_{75}(C_{0.6}B_{0.4})_{25}$ is shifted to the values of ≈ 215 and 230 kOe, respectively (curves *5*–*7*). During annealing with $T_{ann} \geq 600\,^{\circ}C$ in such alloys, the formation of a new phase becomes energetically favorable, with the maximum of the function $P(H)$ near the field range of 280–290 kOe (Figure 5, *c* and *d*, curves *6*–*8*). The new phase corresponds to the phase $Fe_{23}(C,B)_6$ according to the X-ray data (Table 1). The maximum content of this phase in the alloy was obtained after annealing at $T_{ann} = 800\,^{\circ}C$. At the same time, hyperfine magnetic fields H on iron nuclei of phase $Fe_{23}(C,C)_6$ of alloys $Fe_{75}(C_{0.8}B_{0.2})_{25}$ and $Fe_{75}(C_{0.6}B_{0.4})_{25}$ are ≈ 283 and 289 kOe, respectively.

It is known that in cast steels, from the point of view of microstructure, the formation of the phase $Fe_{23}(C,B)_6$ begins with the formation of an nucleus (seed crystal) occurring at the interface between phases α-Fe and $Fe_3(C,B)$ [8]. In this case, the reaction $Fe_3(C,B) + Fe \rightarrow$

Table 2. Intervals of hyperfine magnetic fields H of functions $P(H)$ of phases (ferrite, $Fe_3(C,B)$, $Fe_{23}(C,B)_6$) and fractions S of Fe atoms in these phases for annealed alloys $Fe_{75}(C_{0.8}B_{0.2})_{25}$ and $Fe_{75}(C_{0.6}B_{0.4})_{25}$

T_{ann}, °C	Phases					
	Ferrite		$Fe_3(C,B)$		$Fe_{23}(C,B)_6$	
	H, kOe	S, %	H, kOe	S, %	H, kOe	S, %
Alloy $Fe_{75}(C_{0.8}B_{0.2})_{25}$						
600	320–338	7	195–265	93	–	–
650	320–340	5	195–270	87	270–302	8
800	–	–	170–260	85	260–305	15
Alloy $Fe_{75}(C_{0.6}B_{0.4})_{25}$						
500	309–343	18	170–271	82	–	–
550	319–349	15	183–278	85	–	–
600	319–340	6	180–271	86	271–302	8
800	320–340	3	184–265	80	265–311	17

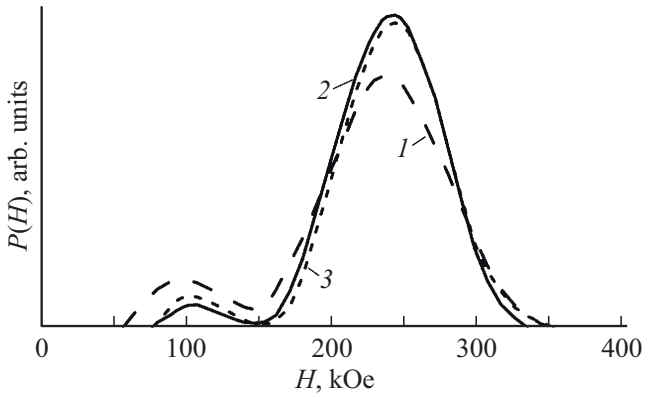

Figure 6. Functions $P(H)$ of amorphous Fe–B alloys with boron content, at.%: 12 (*1*), 13 (it 2), 14 (it3) (Figure 4 in Ref. [34]). The measurement is performed at a room temperature.

$Fe_{23}(C,B)_6$ occurs, during which cementite is consumed, and Fe atoms. The formation of the phase $Fe_{23}(C,B)_6$ due to the decomposition of cementite can be confirmed by data from X-ray diffraction analysis (Table 1), and the Mössbauer study (Table 2).

Table 2 shows the fractions S of Fe atoms contained in the phases $Fe_3(C,B)$, $Fe_{23}(C,B)_6$ and ferrite of alloys with a high boron content at different annealing temperatures. The fractions S were determined by the relative areas under the curves of the functions $P(H)$ of these phases. It follows from the Tables 1 and 2 that the content of both borocementite and ferrite in the alloys decreases during annealing of alloys $Fe_{75}(C_{0.8}B_{0.2})_{25}$ and $Fe_{75}(C_{0.6}B_{0.4})_{25}$ ($T_{ann} \geq 600–650$ °C) with the beginning of the formation of the phase $Fe_{23}(C,B)_6$, which confirms the data given in Ref. [8].

The phase and structural changes occurring during mechanosynthesis and subsequent annealing are also reflected in such magnetic characteristics as the specific saturation magnetization σ_s and the coercive force H_c of alloys. In this case, σ_s of alloys is mainly determined by the phase composition and doping of the phases, and H_c is determined by the structural state of the phases and also by their doping. The dependences $\sigma_s(T_{ann})$ and $H_c(T_{ann})$ of the studied alloys are shown in Figure 7 (curves *2–5*) in comparison with similar dependences of the undoped cementite alloy $Fe_{75}C_{25}$ (dotted curve *1*), produced by the MS method [29].

Let us consider the values of σ_s and H_c of the studied alloys in the post-MS state. It can be seen from Figure 7, *a* that the values of σ_s of boron-containing alloys are higher than the values of σ_s of $Fe_{75}C_{25}$ alloy. This is mainly attributable to the higher content of highly magnetic phases in boron-containing alloys (Table 1) compared with the content of similar phases in the MS alloy $Fe_{75}C_{25}$ [40].

The coercive force of the MS alloy $Fe_{75}C_{25}$ has a value of $H_c \approx 75$ A/cm, which is more than 3 times lower than after annealing at 500 °C (Figure 7, *b*, curve *1*). Such a low value of H_c after MS is mainly attributable to two reasons. Firstly, under the influence of intense plastic deformation during MS, cementite grains become extremely small, that is, they move into the nanoscale range [41]. At the same time, cementite nanograins no longer contain dislocations, however, the cementite crystal lattice is subjected to high residual internal stresses and is strongly distorted, which is reflected in a violation of strict periodicity and the appearance of local changes in lattice parameters throughout the volume of the nanograins [13]. In a strongly distorted cementite lattice, carbon atoms can occupy not only prismatic, in which they are usually found, but also octahedral positions. This circumstance leads to a sharp (by an order of magnitude) decrease in the magnetocrystalline anisotropy constant of MS-cementite and, consequently, to a decrease in its coercive force H_c [42]. Secondly, after MS, the alloy contains a large number of magnetically soft phases (XAP and ferrite) with low H_c.

Let us consider the effect of heat treatment on the change of σ_s and H_c of the studied alloys. During annealing at $T_{ann} < 600$ °C, the distortions of the crystal lattices of cementite and ferrite induced by MS are relieved. The amount of cementite in the alloy increases as a result of the XAP transformation involving unreacted Fe atoms (Table 1). Boron atoms dissolved from the segregations additionally dope cementite. The substitution of highly magnetic phases (XAP and ferrite) with a less magnetic borocementite phase lowers the values of σ_s of the studied alloys in this range of T_{ann} (Figure 7, *a*, curves *4–5*). Similar processes occur in the alloy $Fe_{75}C_{25}$, which also leads to a decrease in the value of its σ_s (Figure 7, *a*, curve *1*).

To clarify the effect of boron on the spesific saturation magnetization, we consider the values of σ_s of the studied alloys after annealing at 500 °C, as a result of which the alloys contain practically only two phases — mainly cementite (borocementite), as well as a small amount of ferrite (Table 1). It follows from Figure 8 that, as the

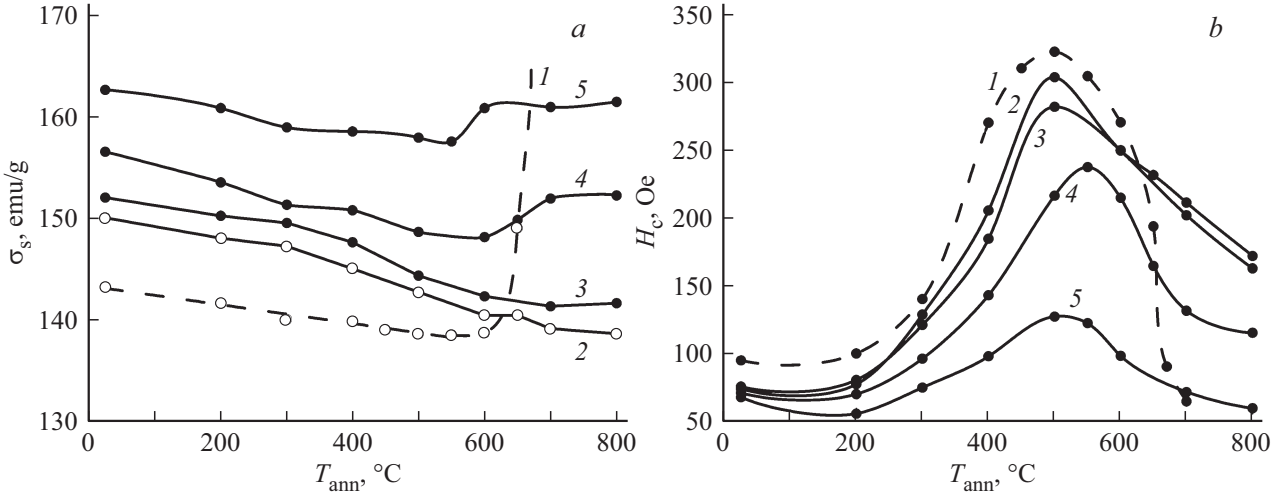

Figure 7. Dependence on the annealing temperature of the specific saturation magnetization σ_s (a) and the coercive force H_c (b) of alloys: *1* — $Fe_{75}C_{25}$ [29], *2* — $Fe_{75}(C_{0.95}B_{0.05})_{25}$, *3* — $Fe_{75}(C_{0.9}B_{0.1})_{25}$, *4* — $Fe_{75}(C_{0.8}B_{0.2})_{25}$ and *5* — $Fe_{75}(C_{0.6}B_{0.4})_{25}$.

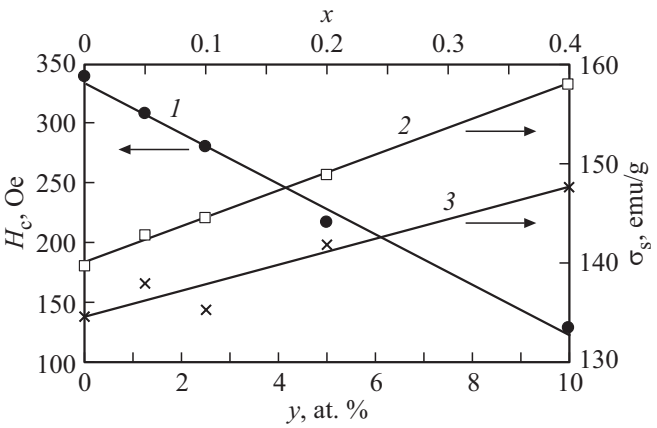

Figure 8. Dependences of the coercive force H_c (*1*), the specific saturation magnetization σ_s (*2*) of alloys and the specific saturation magnetization σ_s of cementite (*3*) of the same alloys on the atomic content y in alloys $Fe_{75}C_{25-y}B_y$ of boron (axis below) or on the fraction of x of boron atoms in the same alloys $Fe_{75}(C_{1-x}B_x)_{25}$ (top axis). The alloys are annealed at $T_{ann} = 500\,^{\circ}C$.

boron content in alloys increases, their values of σ_s linearly increase (Figure 8, curve *2*). Taking into account the fact that boron is almost insoluble in ferrite, the specific saturation magnetization of cementite in these alloys was estimated (Figure 8, curve *3*). The dependence of σ_s of cementite on the boron content in the alloy is also close to linear. This indirectly indicates the substitution of boron atoms for carbon atoms in the cementite lattice, and in proportion to their content in the studied alloys. The data provided in Figure 8 also prove that boron atoms increase the magnetic moment of Fe atoms located in the cementite lattice (Figure 8, curve *3*), which confirms the results of theoretical study in Ref. [39].

Annealing of alloys with increased boron content in the range from 600 to 800 °C leads to the appearance of the $Fe_{23}(C,B)_6$ phase, while the content of ferrite and borocementite in them decreases (Tables 1, 2). The specific saturation magnetization σ_s of the alloy increases at the same time (Figure 7, a, curves *4, 5*). This fact indicates the appearance of a highly magnetic phase in the alloy. This phase $Fe_{23}(C,B)_6$, as its σ_s is higher than the σ_s of borocementite. Undoped cementite Fe_3C undergoes decomposition in case of hourly annealing at a temperature above 600 °C to form α-Fe and graphite (Figure 7, a, curve *1*), as a result of which σ_s of $Fe_{75}C_{25}$ alloy intensively increases. The data shown in Figure 7, a demonstrate the stability of carbide $Fe_{23}(C,B)_6$ up to the maximum annealing temperatures used in this study. The decomposition of carbide into α-Fe and graphite does not occur at $T_{ann} = 800\,^{\circ}C$.

The dependences $H_c(T_{ann})$ of undoped cementite alloy $Fe_{75}C_{25}$ and the studied alloys have a bell-shaped appearance with a maximum at $T_{ann} \approx 500-550\,^{\circ}C$ (Figure 7, b). Let us consider the features of the formation of such a dependence using the example of an alloy $Fe_{75}C_{25}$ (Figure 7, b, curve *1*). One of the reasons for the increase in H_c in the annealing range from 200 to 500 °C is the departure of magnetically soft phases from the alloy composition — the amorphous phase and ferrite — and the formation of cementite based on them. However, the main contribution to the increase and formation of the maximum values of H_c of alloy is made by structural changes in cementite. Cementite becomes a magnetically hard phase after annealing at 500 °C, that is, a phase with an increased value of H_c. This is attributable to the fact that, firstly, as a result of removing distortions of the crystal lattice, a high value of its magnetocrystalline anisotropy constant K, characteristic of undeformed cementite, is restored [42]. Secondly, in deformed powders after such annealing, there is still a sufficiently high density of dislocations and other defects of the crystalline structure, on which, during the

measurement of H_c, the movement of the cementite domain walls is effectively inhibited. It can be seen from the curve *1* in Figure 7, *b* that H_c of cementite decreases after annealing at $T_{ann} > 500-550\,^{\circ}C$, and this is also attributable to a decrease in the density of defects in the crystalline structure of the phases.

The nature of the dependence of $H_c(T_{ann})$ of the studied alloys is determined by the same processes as in the alloy $Fe_{75}C_{25}$. However, the boron content in alloys affects the magnitude of their coercive force. Thus, the maximum values of the coercive force H_c^{max} decrease almost linearly as the boron content in the alloys increases (Figure 7, *b*, and Figure 8). Moreover, alloys after annealing at 500 °C consist mainly of cementite (borocementite) and a small amount of ferrite (Table 1). Since boron is almost insoluble in ferrite at room temperature, it can be assumed that the main amount of boron is found in cementite alloys. Based on experimental data on reducing the coercive force of boron-containing alloys, it can be assumed that boron doping lowers the constant of the magnetocrystalline anisotropy of the carbide phases.

In general, high-temperature annealing completes the processes of doping carbide phases with boron, and there is an intensive decrease in the density of defects in the crystalline structure of the phases, which further reduces the H_c of the studied alloys (Figure 7, *b*, curves *2–5*).

4. Conclusion

1. An X-ray amorphous phase and nanocrystalline cementite with a distorted crystal lattice are formed in the process of mechanosynthesis of $Fe_{75}(C_{1-x}B_x)_{25}$ alloys, where $x = 0.05-0.40$. The alloys also contain some ferrite and boride Fe_2B.

2. Mössbauer measurements have shown that after mechanosynthesis, the X-ray amorphous phase of $Fe_{75}(C_{1-x}B_x)_{25}$ alloys is heterogeneous. In this phase, there are areas of the immediate environment enriched and depleted in metalloid elements, which is reflected in the form of its function $P(H)$. The function has two maxima, one of which is in the range of hyperfine magnetic fields from 90 to 150 kOe, the other is in the range of fields from 180 to 300 kOe.

3. The features of the redistribution of boron in the phases of alloys both in the state after mechanosynthesis and after annealing are investigated. With the exception of the $Fe_{75}(C_{0.6}B_{0.4})_{25}$ alloy, cementite is very weakly doped with boron during mechanosynthesis, the main stage of doping occurs during annealing above a temperature of 400 °C. In an alloy with a high boron content $Fe_{75}(C_{0.6}B_{0.4})_{25}$, some doping with this element occurs already during mechanosynthesis. The Curie temperature of cementite increases in the studied alloys with atomic boron content up to 10 at.% annealed at a temperature of 800 °C with an increase in the boron content in its composition from 210 to 360 °C.

4. $Fe_{23}(C,B)_6$ phase is formed due to cementite and Fe atoms in alloys with high boron content $Fe_{75}(C_{0.8}B_{0.2})_{25}$ and $Fe_{75}(C_{0.6}B_{0.4})_{25}$ during annealing at $T_{ann} \geq 600-650\,^{\circ}C$. Moreover, the higher the boron content in the alloy, the lower the annealing temperature at which this phase is formed.

5. Magnetic measurements have shown that the specific saturation magnetization σ_s of cementite increases linearly with its doping with boron in alloys annealed at $T_{ann} = 500\,^{\circ}C$ $Fe_{75}(C_{1-x}B_x)_{25}$. The dependence $H_c(T_{ann})$ of the studied alloys has a bell-shaped appearance with a maximum at $T_{ann} = 500-550\,^{\circ}C$. The maximum values of the coercive force of alloys decrease linearly as the boron content in the alloys increases. A decrease in H_c of alloys may indirectly indicate a decrease in the magnetocrystalline anisotropy constant K of cementite as it is doped with boron.

Acknowledgments

The authors would like to thank A.I. Golovkova for conducting the X-ray diffraction analysis.

Funding

The study was performed using the equipment of the Shared Use Center „Center of Physical and Physicochemical Methods of Analysis and Study of Properties and Characteristics of the Surface, Nanostructures, Materials and Products“ of the Udmurt Federal Research Center of the Ural Branch of RAS within the framework of the state assignment of the Ministry of Science and Higher Education of the Russian Federation (No. of state registration 124021900079-9).

Conflict of interest

The authors declare that they have no conflict of interest.

References

[1] O. Ozdemir, M. Usta, C. Bindal, A.H. Ucisik. Vacuum **80**, *11–12*, 1391 (2006). DOI: 10.1016/j.vacuum.2006.01.022
[2] G.V. Samsonov, T.I. Serebryakova, V.A. Neronov. Boridy. Atomizdat, M. (1975). p. 376 (in Russian).
[3] X. Chen, Y. Li. Mater. Sci. Eng. A **528**, 770 (2010). DOI: 10.1016/j.msea.2010.09.092
[4] Z. Liu, Y. Li, X. Chen, K. Hu. Mater. Sci. Eng. A **486**, *1–2*, 112 (2008). DOI: 10.1016/j.msea.2007.10.017
[5] Diagramma sostoyaniya dvojnykh metallicheskikh sistem: Spravochnik: V 3-kh t.: Vol. 1. / Pod. red. N.P. Lyakishev. Mashinostroenie, M. (1996). p. 992 (in Russian).
[6] H. Berns, A. Saltykova, A. Röttger, D. Heger. Steel Res. Int. **82**, *7*, 786 (2011). DOI: 10.1002/srin.201000255
[7] J. Lentz, A. Röttger, W. Theisen. Acta Mater. **99**, 119 (2015). DOI: 10.1016/j.actamat.2015.07.037
[8] J. Lentz, A. Röttger, W. Theisen. Acta Mater. **119**, 80 (2016). DOI: 10.1016/j.actamat.2016.08.009
[9] J. Lentz, A. Röttger, W. Theisen. Mater. Charact. **135**, 192 (2018). DOI: 10.1016/j.matchar.2017.11.012

[10] F. Li, Z. Li. J. Alloys Compd. **587**, 267 (2014). DOI: 10.1016/j.jallcom.2013.10.173
[11] P. Acosta, J.A. Jimenez, G. Frommeyer, O.A. Ruano. Mater. Sci. Eng. A **206**, *2*, 194 (1996). DOI: 10.1016/0921-5093(95)10001-6
[12] M.-W. Wu, Y.-C. Fan, H.-Y. Huang, W.-Z. Cai. Metall. Mater. Trans. A **46**, 5285 (2015). DOI: 10.1007/s11661-015-3096-9
[13] R.A. Andrievsky, A.V. Ragulya. Nanokristallicheskie materialy. Academia, M. (2005). p. 192 (in Russian).
[14] R.Z. Valiev, I.V. Alexandrov. Nanostrukturnye metally, poluchennye intensivnoj plasticheskoj deformatsiej. „Logos", M. (2000). p. 272 (in Russian).
[15] C. Suryanarayana. Mechanical alloying and milling. Marcel Dekker Inc, N.Y. (2004). 466 p.
[16] E.P. Yelsukov, G.A. Dorofeev. J. Mat. Sci. **39**, 5071 (2004). DOI: 10.1023/B:JMSC.0000039187.46158.f6
[17] V.A. Barinov, V.I. Voronin, V.T. Surikov, V.A. Kazantsev, V.A. Tsurin, V.V. Fedorenko, S.I. Novikov. Phys. Met. Metallogr. **100**, *5*, 456 (2005).
[18] V.A. Volkov, I.A. Yelkin, A.A. Chulkina, S.N. Paranin, V.V. Tarasov, I.S. Trifonov. Khimicheskaya fizika i mezoskopiya **19**, *1*, 67 (2017). (in Russian).
[19] E.V. Shelekhov, T.A. Sviridova. Met. Sci. Heat Treat. **42**, *8*, 309 (2000). DOI: 10.1007/BF02471306
[20] E.V. Voronina, N.V. Ershov, A.L. Ageev, Yu.A. Babanov. Phys. Status Solidi B **160**, *2*, 625 (1990). DOI: 10.1002/pssb.2221600223
[21] E.P. Yelsukov, G.A. Dorofeev. Hyperfine Interact. **164**, 51 (2005). DOI: 10.1007/s10751-006-9233-5
[22] T.A. Sviridova, E.V. Shelekhov, V.I. Bazilyan, T.R. Chueva, N.V. Shvyndina, N.P. Dyakonova. J. Alloys Compd. **586**, S73 (2014). DOI: 10.1016/j.jallcom.2012.10.118
[23] E.N. Sheftel, V.A. Tejetov, F.V. Kiryukhantsev-Korneev, E.V. Kharin, G.S. Usmanova, O.M. Zhigalina. Izvestiya vuzov. Poroshkovaya metallurgiya i funktsional'nye pokrytiya **3**, 65 (2020) (in Russian). DOI: 10.17073/1997-308X-2020-3-65-75
[24] A.A. Rempel, A.I. Gusev. Phys. Solid State **42**, *7*, 1280 (2000).
[25] L.E. Karkina, N.I. Medvedeva, I.L. Yakovleva. Materialovedenie, **5**, 40 (2005) (in Russian).
[26] M.E. Nicholson. JOM **9**, 1 (1957). DOI: 10.1007/BF03398435
[27] M.E. Nicholson. Trans. Met. Soc. **209**, 1 (1957).
[28] O.Yu. Gutina, N.I. Medvedeva, I.R. Shein, A.L. Ivanovskii, J.E. Medvedeva. Phys. Status Solidi B **246**, *9*, 2167 (2009). DOI: 10.1002/pssb.200945064
[29] A.A. Chulkina, A.I. Ulyanov, A.L. Ulyanov, I.A. Baranova, A.V. Zagainov, E.P. Yelsukov. Phys. Metals Metallogr. **116**, *1*, 19 (2015). DOI: 10.1134/S0031918X14100056
[30] E.P. Elsukov, A.L. Ul'yanov, D.A. Vytovtov. Bull. Russ. Acad. Sci.: Phys. **71**, *9*, 1253 (2007). DOI: 10.3103/S1062873807090134
[31] E.P. Elsukov, G.A. Dorofeev, A.L. Ul'yanov, D.A. Vytovtov. Physics of Metals and Metallography **102**, *1*, 76 (2006). DOI: 10.1134/S0031918X06070106
[32] E.P. Yelsukov, G.A. Dorofeev, A.V. Zagainov, N.F. Vildanova, A.N. Maratkanova. Mater. Sci. Eng. A **369**, *1–2*, 16 (2004). DOI: 10.1016/j.msea.2003.08.054
[33] E.P. Elsukov, I.V. Povstugar, A.L. Ul'yanov, G.A. Dorofeev. Phys. Met. Metallogr. **101**, *2*, 174 (2006). DOI: 10.1134/S0031918X06020116
[34] R. Oshima, F.E. Fujita. Jap. J. Appl. Phys. **20**, *1*, 1 (1981). DOI: 10.1143/JJAP.20.1
[35] C.C. Cao, Y.G. Wang, G.T. Xia, L. Zhu, Y. Meng, X.B. Zhai. EPL **118**, *6*, 67007 (2017). DOI: 10.1209/0295-5075/118/67007
[36] C.C. Cao, Y.G. Wang, L. Zhu, Y. Meng, Y.D. Dai, J.K. Chen. J. Alloys Compd. **722**, 394 (2017). DOI: 10.1016/j.jallcom.2017.06.147
[37] E.M. Kutashova, A.V. Pyataev, N.F. Shkodich, A.S. Rogachev, Yu.B. Scheck JMMM **492**, 165663 (2019). DOI: 10.1016/j.jmmm.2019.165663
[38] X.-W. Liu, S. Zhao, Y. Meng, Q. Peng, A.K. Dearden, C.-F. Huo, Y. Yang, Y.-W. Li, X.-D. Wen. Sci. Rep. **6**, 26184 (2016). DOI: 10.1038/srep26184
[39] N.I. Medvedeva, I.R. Shein, O.Yu. Gutina, A.L. Ivanovskiĭ. Phys. Solid State **49**, *12*, 2298 (2007). DOI: 10.1134/S106378340712013X
[40] E.P. Yelsukov, G.A. Dorofeev, V.M. Fomin. J. Metastable Nanocryst. Mater. **15–16**, 445 (2003). DOI: 10.4028/www.scientific.net/JMNM.15-16.445
[41] E.P. Yelsukov, A.I. Ul'yanov, A.V. Zagainov, N.B. Arsent'yeva. J. Magn. Magn. Mater. **258–259**, 513 (2003). DOI: 10.1016/S0304-8853(02)01129-0
[42] A.K. Arzhnikov, L.V. Dobysheva, C. Demangeat. Phys.: Condens. Matter **19**, *19*, 196214 (2007). DOI: 10.1088/0953-8984/19/19/196214

Translated by A.Akhtyamov